PHYSICAL REVIEW B **80**, 020401(R) (2009)

# Probing electronic-phase-separated insulating domains in the metallic phase of patterned perovskite manganite microwires

T. Nakajima,[1,*] T. Tsuchiya,[1] Y. Ueda,[2] and T. Kumagai[1]
[1]*National Institute of Advanced Industrial Science and Technology, Tsukuba, Ibaraki 305-8565, Japan*
[2]*Institute for Solid State Physics, University of Tokyo, Kashiwa, Chiba 277-8515, Japan*
(Received 6 April 2009; revised manuscript received 12 June 2009; published 8 July 2009)

We investigated the mesoscopic electrical transport properties of micropatterned perovskite manganite ($La_{0.5}Ba_{0.5}MnO_3$; LBMO) films that show electronic phase separation between ferromagnetic and *A*-type antiferromagnetic phases. The patterned-wire LBMO film of 10 $\mu$m width showed an insulator-metal (IM) transition associated with a ferromagnetic transition, followed by re-emergence of insulator characteristics below 200 K that did not appear in the unpatterned thin films. By controlling wire width, we were able to probe the phase-separated antiferromagnetic insulating domains, where large first-order IM transitions appeared in the patterned narrow wire with a small channel. Our results show that probing small population of insulating domains in metallic phases and their control by magnetic fields depends strongly on the dimensions of the microchannel.

DOI: 10.1103/PhysRevB.80.020401 PACS number(s): 75.47.Lx, 73.50.−h, 75.47.Gk, 73.23.−b

The electronic phase-separation (EPS) state near the phase boundary between a ferromagnetic (FM) metal and an antiferromagnetic (AFM) insulator, as seen in hole-doped perovskite manganites ($R_{1-x}A_xMnO_3$, *R*: rare-earth elements and *A*: Ca, Sr, and Ba), is a crucial phenomenon for understanding external-field-induced phase transitions such as the colossal magnetoresistance (CMR) effect.[1,2] There are many reports of experimental and theoretical studies on the EPS state of manganites in bulk and in thin-film materials.[3–5] The phase-separated domains in these materials are generally from a few nanometers to micrometers in size, and their resistive responses can be controlled by changing the population and the size of the metallic and the insulating microdomains.[3–8] From an engineering perspective, there are two problems that are related to the colossal resistive response of manganites and need to be solved: (1) it is difficult to produce a large magnetoresistance (MR) response at room temperature and (2) a strong magnetic field is required for the emergence of the MR effect. Although we have overcome the first of these problems by successfully generating 1000% CMR response at room temperature under 9 T in the *A*-site ordered manganites that realized the EPS state above room temperature,[8–10] the second problem has not yet been solved.

Recent studies focusing on the EPS state of microscopic transport properties of manganites have used thin-film materials artificially patterned at submicron–micron sizes.[11–15] The results of these studies enable dynamic and precise control of resistive switching properties, including the low-field magnetoresistance (LFMR) effect. These studies have included investigation of $(La_{1-y}Pr_y)_{1-x}Ca_xMnO_3$ (LPCMO), which exhibits an EPS state between the ferromagnetic metal and the charge-ordered (CO) insulating phases.[1] Singh-Bhalla *et al.* reported an intrinsic tunneling effect and the LFMR effect in submicron-size bridges composed of LPCMO.[16] For a valid manipulation of physical properties in microfabricated manganites, and to explore the possibilities of EPS domain engineering, a further understanding of the mesoscopic-scale relationship between the coherent length of EPS domains and the probe size is needed.

In this study, we investigated the microscopic electrical transport properties of epitaxial $La_{0.5}Ba_{0.5}MnO_3$ (LBMO) films. A bulk polycrystalline LBMO shows a ferromagnetic metal transition at around 270 K as reported in previous studies.[17,18] In our study, powder neutron-diffraction measurements at low temperature [Fig. 1(a)] revealed that the LBMO contained *A*-type AFM domains in the FM metal phase. The weak magnetic Bragg peak $(00\frac{1}{2})$ corresponding to the *A*-type AFM phase appeared at around $2\theta=13.2°$ below 150 K [Fig. 1(b)], indicating that the submicrometer-scale *A*-type AFM domains were coexistent with the FM phase. The *A*-type AFM phase in the manganites showed metallic behavior in the *ab* plane and insulating behavior along the *c* axis. The in-plane (*ab*) and the out-of-plane (*c*) resistivities of *A*-type AFM in the manganite single crystals at low temperature were on the orders of $10^{-2}$ and $10^2$ $\Omega$ cm, respectively.[19] Thus, the randomly distributed *A*-type AFM microdomains in the phase-separated FM metal of the LBMO are weak insulators compared to the phase-separated CO domains of high resistivity ($\sim 10^5$ $\Omega$ cm) in the LPCMO. We focused on the EPS state between the metallic FM phase and the weak insulating *A*-type AFM domains and studied the probe-size dependence of electrical

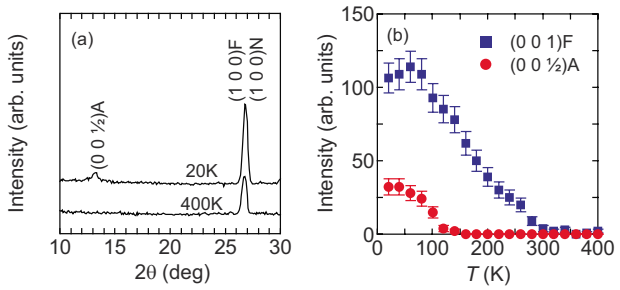


FIG. 1. (Color online) (a) Neutron diffraction patterns of polycrystalline LBMO at 400 and 20 K, indexed to the simple perovskite unit cell, where subscripts N, F, and A represent nuclear, FM, and *A*-type AFM, respectively. (b) Temperature dependence of magnetic diffractions for $(001)_F$ and $(00\frac{1}{2})_A$.

 

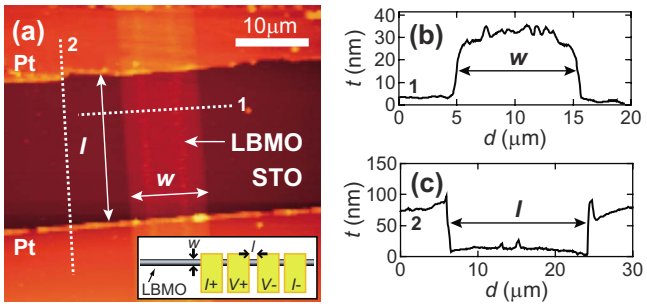


FIG. 2. (Color online) (a) AFM image of the LBMO wire and deposited Pt contacts for the $\rho$ measurements, where $w$ and $l$ represent wire width and probe contact distance, respectively. The inset shows the measurement configuration. Cross sections of (b) patterned wire [line 1 on panel (a)] and (c) valley between the probe contacts [line 2 on panel (a)].

transport properties of the LBMO with artificial microwire geometry.

We employed an excimer laser-assisted metal organic deposition (ELAMOD) process based on a chemical solution deposition to fabricate micropatterned perovskite manganite films. The ELAMOD process has a big advantage over other methods for the patterning of oxide materials, such as the focused ion-beam physical etching process. It is a simple process that does not damage the film during patterning because the oxide films are crystallized after patterning.[20,21] The preparation of LBMO began by mixing 2-ethylhexanoate solutions of the constituent metals diluted with toluene. The La:Ba:Mn molar ratio in the coating solution was 0.5:0.5:1.0. This solution was spin coated onto a $SrTiO_3(100)$ substrate at 4000 rpm for 10 s. The coated films were irradiated by a KrF laser (Lambda Physik, Compex 110) in two steps. In the first step, laser irradiation was carried out at a fluence of 25 $mJ/cm^2$ for 4000 pulses at room temperature through a chromium photomask. The laser-irradiated regions (wire shape) were solidified by decomposing the organic components, and patterned films with the wire geometry were obtained by the removal of unirradiated parts by acetone. The patterned films were then heated to 500 °C in air for 10 min, and then irradiated a second time with a KrF laser at a fluence of 80 $mJ/cm^2$ for 20 000 pulses at 500 °C in air. The films so obtained were annealed in air at 700 °C for 30 min to eliminate any slight oxygen vacancies generated at the film surface. Details of the crystal-growth mechanism of the ELAMOD process are described elsewhere.[21] By means of this process, we successfully obtained micropatterned LBMO with the wire geometry, which we confirmed by atomic force microscopy analysis [Fig. 2(a)]. The relationship between electrical resistivity ($\rho$) and temperature of the samples was determined by dc four-probe transport measurements [inset in Fig. 2(a)]. The multiple experimental runs for $\rho$-$T$ curve of each sample were continuously measured under identical probing conditions. The patterned film thickness ($t$), the wire width ($w$), and the probe contact distance ($l$) were checked by atomic force microscopy. The film thickness for each sample in this study was 30 nm.

The $\rho$-$T$ curves for various wire patterns (Fig. 3) show

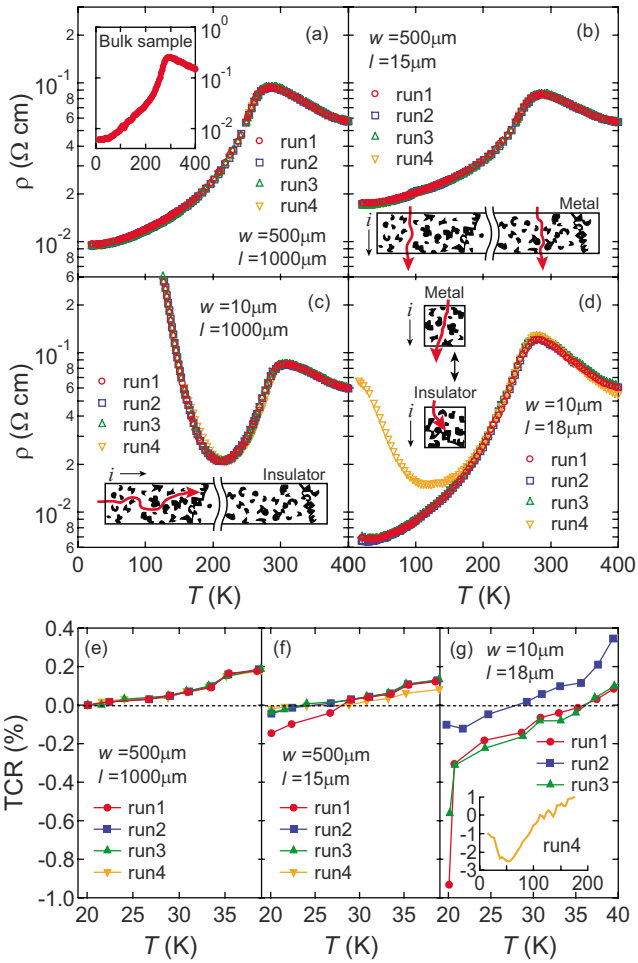


FIG. 3. (Color online) $\rho$-$T$ curves for patterned wires of dimensions (a) $w$=500 $\mu$m and $l$=1000 $\mu$m, (b) $w$=500 $\mu$m and $l$=15 $\mu$m, (c) $w$=10 $\mu$m and $l$=1000 $\mu$m, and (d) $w$=10 $\mu$m and $l$=18 $\mu$m. Multiple measurement runs for each sample were carried out under the same probe conditions. The inset in panel (a) shows $\rho$-$T$ curve of bulk polycrystalline LBMO. Schematic models [insets in panels (b)–(d)] show conduction pathways in the EPS state of LBMO. White represents FM metal and black represents AFM insulator. TCR variations at low temperatures for the patterned wires of dimensions (e) $w$=500 $\mu$m and $l$=1000 $\mu$m, (f) $w$=500 $\mu$m and $l$=15 $\mu$m, and (g) $w$=10 $\mu$m and $l$=18 $\mu$m.

that for the LBMO film with a wire geometry of $w$=500 $\mu$m and $l$=1000 $\mu$m [Fig. 3(a)], the IM transition occurred at 270 K, which is consistent with the ferromagnetic metal transition of bulk LBMO. This shows that the electric resistivity of this sample was almost the same as that of bulk material. From second to fourth experimental runs for this sample reproducibly exhibited identical $\rho$-$T$ curves to that of the first run. This $\rho$-$T$ behavior was not changed at all in the further measurement runs. In the system in which a FM phase dominantly governed the matrix, there must be many conduction paths in a sample with large $w$ and long $l$, even if small AFM domains are emerged. Therefore, the observed resistivity represents an averaged low value and then behaves as simply metallic down to low temperature at around 20 K as shown in the temperature coefficient of resistance (TCR) data [Fig. 3(e)].

In the sample with a wire width of 500 $\mu$m and a short contact distance ($l=15$ $\mu$m), a slight variability in the resistivity at low temperatures was evident. The metallic behavior was roughly the same in the four experimental runs [Fig. 3(b)]: the variation in $\rho$ values at 20 K in each measurement remained only within 4%. However, the TCR values changed from positive to negative at different temperatures below 30 K for each experimental run [Fig. 3(f)]. We consider that the negative TCR is responsible not for resistive grain boundaries (RGBs) in the wire films but for intrinsic EPS. If the RGB effect is dominant for the $\rho$ behaviors at low temperature in this system, it would influence $\rho$ for the large sampling dimensions ($w=500$ $\mu$m and $l=1000$ $\mu$m) with numbers of RGBs to a greater degree than the $\rho$ for the small measurement geometry with fewer grains. A negative TCR indicates an effective increase in the size of the insulating domains between the probe contacts. It appears that for short probe distances the resistivity is more likely to be affected by emerging antiferromagnetic insulating domains than is the case for larger probing dimensions. On the contrary, in the narrow wire sample ($w=10$ $\mu$m and $l=1000$ $\mu$m) [Fig. 3(c)], we observed a metal-insulator (MI) transition at around 200 K, some 70 K below the insulator-metal (IM) transition at 270 K, and the observed data were consistent for each experimental run. The increases in resistivity were attributed to the emerging phase-separated antiferromagnetic domains. The reason why the MI transition appeared in this case can be easily understood from the schematic illustrations provided as insets in Figs. 3(b) and 3(c). The metallic conduction paths are readily available when the probe contacts are sufficiently wide ($w\sim500$ $\mu$m). However, barriers to electron hopping because of connections between discrete submicron-size insulating AFM domains in the ferromagnetic metal phase could emerge anywhere along the long contact length ($l\sim1000$ $\mu$m) in the case of the narrow wire ($w\sim10$ $\mu$m) sample. This suggests that even minor insulating AFM domains in the phase-separated state can be effective in the narrow wire structure. For an LBMO wire of narrow width and short contact distance ($w=10$ $\mu$m, $l=18$ $\mu$m) [Fig. 3(d)], the $\rho$-$T$ curves for all runs trend upward below the IM transition at 270 K, but a large increase in resistivity at low temperature is notable in run 4. These increases in resistivity were caused by the disconnection of metallic paths by emerging antiferromagnetic domains, as seen in Figs. 3(b) and 3(c). For the LBMO wires of narrow width and short contact distance [Fig. 3(d)], a large difference of $\rho$-$T$ behaviors between runs 1 and 4 is noteworthy below 200 K. Not only does run 4 show an obvious MI transition at 110 K, but for runs 1–3, the temperatures at which TCR values change from positive to negative differ by 28–36 K, and negative TCR values at 20 K are scattered in the range from −0.1% to −1.0% [Fig. 3(g)]. This indicates that the observed resistivity behaviors for LBMO wires of these dimensions (10 $\mu$m$\times$18 $\mu$m$\times$30 nm) are determined by the position and the size of randomly emerging antiferromagnetic domains, and that the resistivity can be affected by very small numbers of antiferromagnetic domains. Thus, the anomalous increase in resistivity as seen in run 4 would accidentally appear only when the AFM domains strongly shut metallic pathways in small probing matrix. Actually, we observed this peculiar behavior of large resistivity increase in approximately 10% of measurement runs. This result also means that the emergence sites of AFM domain were not pinned in the materials.

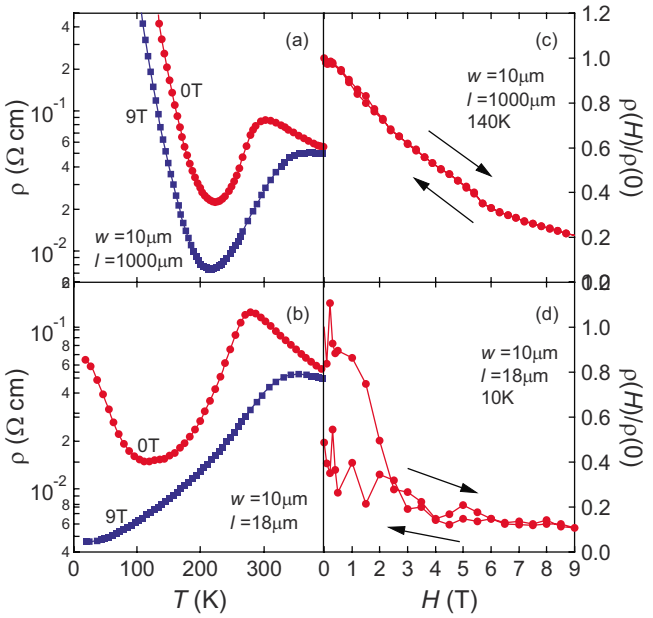


FIG. 4. (Color online) $\rho$-$T$ curves under 0 and 9 T for patterned wires of dimensions (a) $w=10$ $\mu$m and $l=1000$ $\mu$m and (c) $w=10$ $\mu$m and $l=18$ $\mu$m. $\rho(H)/\rho(0)$ curves showing an MR effect for patterned wires of dimensions (b) $w=10$ $\mu$m and $l=1000$ $\mu$m and (d) $w=10$ $\mu$m and $l=18$ $\mu$m.

We also investigated the dependence of MR properties on probe contact distance for the narrow LBMO wires. Figure 4(a) shows the magnetic field ($H$) dependence of $\rho$-$T$ curves of LBMO wires with $l=1000$ $\mu$m. The long contact distance prevented the formation of metallic paths even under a strong magnetic field ($H=9$ T). The magnetic field dependence $[\rho(H)/\rho(0)]$ for this sample at 140 K showed no first-order IM transition [Fig. 4(b)]; the resistivity simply decreased with increasing $H$ (the MR effect could not be measured at temperatures lower than 140 K because of the high resistance of the sample). On the contrary, the MR effect was clearly observed in the LBMO wire when measured with short contact length ($l=18$ $\mu$m) [Fig. 4(c)]. The increased resistivity at low temperatures was suppressed by the applied magnetic field, and the $\rho$-$T$ curve demonstrated metallic behavior under 9 T. The magnetic field dependence $[\rho(H)/\rho(0)]$ as a function of $H$ showed a first-order IM transition with the application of a small magnetic field, namely, the LFMR effect: the $\rho(H)/\rho(0)$ ratio started to drop dramatically when the applied magnetic field reached 1.0 T and approached its minimum value (about 0.15) at 2.5–4 T [Fig. 4(d)]. It appears that the LFMR effect occurred in this sample because the collapse of a remarkably small population of AFM domains, in response to the applied magnetic field in the small channel, produced an on-off action for resistivity. The first-order IM transition under a low magnetic field was also observed in an LPCMO that exhibited a phase separation with a charge-ordered state in a smaller sampling dimension ($w=0.5$ $\mu$m) than that of our observations

($w=10$ $\mu$m).[14,16] This indicates that discrete *A*-type AFM domains with a higher mobility of carrier electrons than that of the CO state are more sensitive to magnetic fields, resulting in the IM transition in the 20 times larger probing size of the EPS state between the FM and the CO phases.

The MR effect of the LBMO wire with short contact length ($l=18$ $\mu$m) can be seen in Fig. 4(d): the $\rho(H)/\rho(0)$ curve loses its smooth form below 3.0 T. We consider this behavior to be an intrinsic characteristic of the conduction properties of the EPS manganites. As the magnetic field decreases, the metallic pathways appear to be disrupted by the re-emergence of insulating AFM domains, but the conductivity did not change gradually because the re-emergent insulating domains were heterogeneously distributed in the FM phase. Consequently, the resistivity changes observed at small channel were not smooth, but showed considerable scatter.

In addition, the MR curve measured for the small-probe dimension [Fig. 4(b)] did not trace the resistivity curve before applying the magnetic field [run 4 of Fig. 3(d)]. This proved that the insulating domains were not pinned in this system. It appears that LBMO contains only a small amount of slightly distorted cubic material and thus the emergence sites of AFM domains tend not to be strictly determined to the same positions. To make electrical transport properties reproducible in LBMO, minimal distortion, such as ion doping or artificial damage, might effectively pin the active sites of AFM domains.

We investigated the mesoscopic electrical transport properties of micropatterned perovskite manganite LBMO films that show EPS between FM and *A*-type AFM phases. The patterned wires were fabricated by the ELAMOD process. A patterned wire of LBMO film of 10 $\mu$m width showed an IM transition associated with ferromagnetic transition that was followed by a re-emergent insulator transition below 200 K that did not appear in unpatterned thin films. Through the control of wire width, we were able to probe phase-separated antiferromagnetic insulating domains and demonstrated a large first-order IM transition in the patterned narrow wire with a small channel. Our study showed that probing of the insulating domains as minor phase in the metallic phases, and their control by magnetic fields, is strongly dependent on microchannel dimensions.

The authors acknowledge T. Yamauchi at the University of Tokyo for fruitful discussions.

*t-nakajima@aist.go.jp

[1] M. Uehara, S. Mori, C. H. Chen, and S.-W. Cheong, Nature (London) **399**, 560 (1999).
[2] E. Dagotto, T. Hotta, and A. Moreo, Phys. Rep. **344**, 1 (2001).
[3] N. Fukumoto, S. Mori, N. Yamamoto, Y. Moritomo, T. Katsufuji, C. H. Chen, and S.-W. Cheong, Phys. Rev. B **60**, 12963 (1999).
[4] R. Kajimoto, H. Yoshizawa, H. Kawano, H. Kuwahara, Y. Tokura, K. Ohoyama, and M. Ohashi, Phys. Rev. B **60**, 9506 (1999).
[5] J. Burgy, M. Mayr, V. Martin-Mayor, A. Moreo, and E. Dagotto, Phys. Rev. Lett. **87**, 277202 (2001).
[6] Z. P. Luo, D. J. Miller, and J. F. Mitchell, J. Appl. Phys. **105**, 07D528 (2009).
[7] S. Mori, T. Katsufuji, N. Yamamoto, C. H. Chen, and S.-W. Cheong, Phys. Rev. B **59**, 13573 (1999).
[8] Y. Ueda and T. Nakajima, Prog. Solid State Chem. **35**, 397 (2007).
[9] T. Nakajima and Y. Ueda, J. Appl. Phys. **98**, 046108 (2005).
[10] T. Nakajima and Y. Ueda, Physica B **378-380**, 520 (2006).
[11] N. D. Mathur, G. Burnell, S. P. Isaac, T. J. Jackson, B.-S. Teo, J. L. MacManus-Driscoll, L. F. Cohen, J. E. Evetts, and M. G. Blamire, Nature (London) **387**, 266 (1997).
[12] T. Wu and J. F. Mitchell, Appl. Phys. Lett. **86**, 252505 (2005).
[13] R.-W. Li, T. Kanki, H. Tohyama, M. Hirooka, H. Tanaka, and T. Kawai, Nanotechnology **16**, 28 (2005).
[14] Y. Yanagisawa, H. Tanaka, T. Kawai, and L. Pellegrino, Appl. Phys. Lett. **89**, 253121 (2006).
[15] T. Z. Ward, S. Liang, K. Fuchigami, L. F. Yin, E. Dagotto, E. W. Plummer, and J. Shen, Phys. Rev. Lett. **100**, 247204 (2008).
[16] G. Singh-Bhalla, S. Selcuk, T. Dhakal, A. Biswas, and A. F. Hebard, Phys. Rev. Lett. **102**, 077205 (2009).
[17] F. Millange, V. Caignaert, B. Domengès, and B. Raveau, Chem. Mater. **10**, 1974 (1998).
[18] T. Nakajima, H. Yoshizawa, and Y. Ueda, J. Phys. Soc. Jpn. **73**, 2283 (2004).
[19] H. Kuwahara, T. Okuda, Y. Tomioka, A. Asamitsu, and Y. Tokura, Phys. Rev. Lett. **82**, 4316 (1999).
[20] T. Tsuchiya, T. Yoshitake, Y. Shimakawa, I. Yamaguchi, T. Manabe, T. Kumagai, Y. Kubo, and S. Mizuta, Jpn. J. Appl. Phys., Part 2 **42**, L956 (2003).
[21] T. Nakajima, T. Tsuchiya, M. Ichihara, H. Nagai, and T. Kumagai, Chem. Mater. **20**, 7344 (2008).